Structure, spin dynamics, and magnetic properties of annealed nanoscale Fe layers on GaAs

Justin M. Shaw[a)]
National Institute of Standards and Technology, Boulder, Colorado 80305

Charles M. Falco
College of Optical Sciences, University of Arizona, Tucson, Arizona 85721

(Received 28 August 2006; accepted 29 November 2006; published online 2 February 2007)

We performed a detailed study of the effect of annealing (at temperatures up to 300 °C) on 0.2–3.0 nm thick epitaxial Fe layers deposited on GaAs(001). Using Brillouin light scattering, we studied the magnetic properties and spin dynamics of these layers and found a strong correlation between magnetic properties and the structure and chemical properties, as measured with electron diffraction, scanning tunneling microscopy, and x-ray photoemission spectroscopy. We found that significant changes in crystallinity and microstructure occur with annealing. Specifically, annealing of the thinnest layers results in the formation of a discontinuous magnetic layer with increased crystal order. At slightly larger thicknesses, faceted pits form in the Fe layer. This change in structure results in an earlier transition to a ferromagnetic phase, the creation of an additional higher frequency spin-wave mode, and a reduction in the magnetic uniaxial anisotropy constant. © *2007 American Institute of Physics*. [DOI: 10.1063/1.2433713]

INTRODUCTION

Epitaxial Fe layers deposited on GaAs(001) substrates have been studied for almost two decades.[1] The driving force behind this interest now resides in the emerging field of spintronics, where the spin degree of freedom is exploited in addition to charge in semiconductor devices. Ferromagnetic layers in contact with a semiconductor can be used to generate a spin-polarized current within the semiconductor. This is referred to as "spin injection." Fe on GaAs shows promise in this area of technology, since epitaxial Fe is relatively easy to grow due to a close lattice match (the lattice constant of Fe is within 1.4% of half the lattice constant of GaAs). Since the Fe is epitaxial, the magnetocrystalline anisotropy can be exploited to orient the magnetization along specific crystallographic directions relative to the semiconductor substrate. In addition, spin injection from Fe into GaAs either from a direct Schottky contact[2] or a quantum well heterostructure[3,4] has been demonstrated, as has spin accumulation at the Fe/GaAs interface.[5]

While extensive work has been conducted on epitaxial Fe on GaAs,[6–12] very little work to date has explored the effect of thermal annealing on this system.[13–17] As we shall show in this paper, thermal annealing can dramatically alter the physical properties of the Fe layer. An understanding of these thermally generated changes in properties is needed to engineer processes to improve device performance. In addition, device fabrication generally requires wafers to undergo several thermal cycles throughout the manufacturing process which can lead to parasitic or undesirable changes in properties. In this paper, we present the results of our extensive study on the effects of postdeposition annealing on Fe layers. During this investigation we discovered that a significant change in structure occurs with annealing, which dramatically influences the magnetic properties and generates an additional spin-wave mode.

EXPERIMENT

We used a four-chamber molecular beam epitaxy (MBE) system with a base pressure in the mid-to-low 10^{-9} Pa (10^{-11} Torr) range for sample growth, *in situ* reflection high energy electron diffraction (RHEED), Auger electron spectroscopy (AES), and x-ray photoemission spectroscopy (XPS). *In situ* XPS data were obtained using a cylindrical mirror analyzer with a resolution of 0.5 eV utilizing a dual anode Mg $K\alpha$ source. *In situ* AES was performed using the same analyzer and a 10 keV electron gun. Surfaces of commercial Si-doped 50 mm GaAs(001) wafers were cleaned under 1 keV Ar^+ (18 mA, 20 mPa) for approximately 80 min with a final temperature of 600 °C, resulting in a smooth and clean (4×6) GaAs(001) reconstructed surface, as shown in Fig. 1(a). AES analysis of this surface indicates that it is free from any contaminants. Fe layers for *in situ* scanning tunneling microscopy (STM) analysis were grown in a second MBE system not equipped with an Ar^+ ion gun, which therefore required surfaces to be cleaned by a wet chemical treatment. This wet chemical treatment consisted of consecutive 10 min ultrasonic baths in high purity acetone and methanol prior to a 2 min immersion in HCl. Surfaces were then sulfur-passivated for 20 min in a 20% aqueous solution of $(NH_4)_2S$ and immediately loaded into the MBE system. The wafers were heated to approximately 600 °C to desorb the S on the surface, which resulted in an intense and streaked (2×1) GaAs RHEED pattern, as shown in Fig. 1(b), suggesting the formation of dimer rows. The difference in magnetic properties of Fe layers grown using both surface preparation methods was found to be minimal. However, we

[a)]Electronic mail: justin.shaw@nist.gov

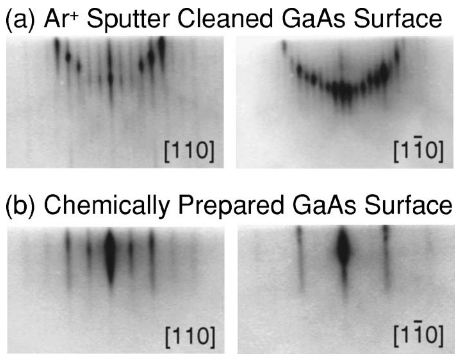

FIG. 1. RHEED images of the initial GaAs(001) surface of the (a) (4×6) GaAs reconstruction from Ar^+ sputter cleaning at high temperature, and (b) (2×1) GaAs reconstruction from a wet chemical treatment followed by a high-temperature anneal.

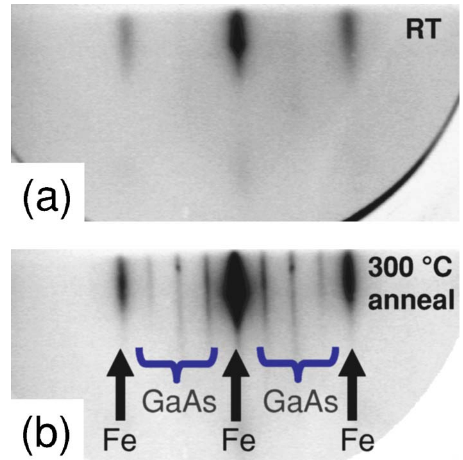

FIG. 2. (Color online) RHEED images of a 0.4 nm Fe layer: (a) as deposited at RT and (b) after a 10 min anneal at 300 °C. Simultaneous diffraction from the Fe and GaAs are present in the annealed image.

do note that small differences in properties are likely since surface roughness and nucleation site density will differ.

Fe layers were deposited using a Knudsen cell at 0.40 nm/min while the rotating substrate was held at 20–40 °C. These rates were calibrated using Rutherford backscattering spectrometry, which does not measure thickness directly. As a result, thicknesses reported here are idealized, calculated using the bulk density of Fe, and more correctly refer to the Fe coverage (areal density) according to the following conversion: $0.143\ \text{nm}=1\text{ML}$(mololayer) $=1.21\times10^{15}\ \text{cm}^{-2}$. After the Fe deposition, the annealed samples were gradually heated to either 200 or 300 °C over 30 min and held at the specified temperature for 10 min. After the samples reached room temperature (RT), we deposited a 5 nm Al overlayer using an e-beam evaporation source for samples that would subsequently undergo *ex situ* analysis.

We performed *ex situ* Brillouin light scattering (BLS) using a diode-pumped Nd:YAG (yttrium aluminum garnet) laser with a wavelength of 532 nm and an output power of 200 mW to probe thermally excited long-wavelength spin-wave modes. We used a 180° backscattering geometry and applied in-plane magnetic fields of up to 1.0 T. Backscattered photons were analyzed with a tandem 6(3+3)-pass Fabry-Pérot interferometer with a frequency resolution of 0.2 GHz and a dark count of 2.2 counts/s. In-plane external magnetic field dependent measurements of the spin-wave frequency were taken along the easy [110] and hard [1$\bar{1}$0] directions. In addition, the spin-wave frequency dependence of the in-plane angle was performed using a fixed in-plane external magnetic field of 0.3 T. We developed a program to simulate and fit these data to determine quantitative values of the effective magnetization and anisotropy constants. The details of the fitting process are described elsewhere.[18] Magneto-optic Kerr effect measurements confirm that the magnetization was in plane for all cases. Therefore, an out-of-plane magnetization was not considered in the BLS analysis.

RESULTS AND DISCUSSION

Structure and chemical properties

The annealing process has a considerable effect on the crystallinity and microstructure of nanoscaled Fe layers on GaAs. The RHEED pattern for a 0.4 nm body centered cubic Fe layer immediately after RT growth is shown in Fig. 2(a). Low intensity diffraction of the 0.4 nm Fe layer is present, showing the Fe has at least partially crystallized and ordered. At this thickness, no evidence of GaAs diffraction is observed. However, after a 300 °C anneal, the intensity of the Fe diffraction increases significantly with superposed GaAs diffraction, as shown in Fig. 2(b). This image indicates that the 0.4 nm Fe layer becomes more ordered and coalesces into larger islands that expose regions of GaAs on the surface during the annealing process.

The RHEED patterns for various Fe layer thicknesses ranging from 0.2 to 1.3 nm are shown in Fig. 3 for the RT deposited and 200 and 300 °C annealed layers. Simultaneous GaAs and Fe diffraction peaks are present in 300 °C annealed Fe layers up to approximately 0.7 nm. Above this thickness only Fe layer diffraction is present; the surface of the Fe is reconstructed. This (2×2) reconstruction is thought to be caused by As on the surface.[6] Annealing Fe layers less than 0.7 nm in thickness to 200 °C also increases the order and island formation, but to a lesser extent. Above 0.7 nm there is little change in the RHEED pattern for the 200 °C annealed and the RT Fe layers.

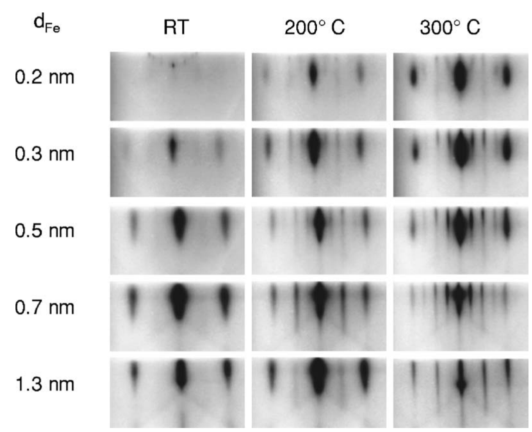

FIG. 3. RHEED images for several thicknesses of Fe for RT as deposited (left column), 200 °C annealed (center column), and 300 °C annealed (right column).

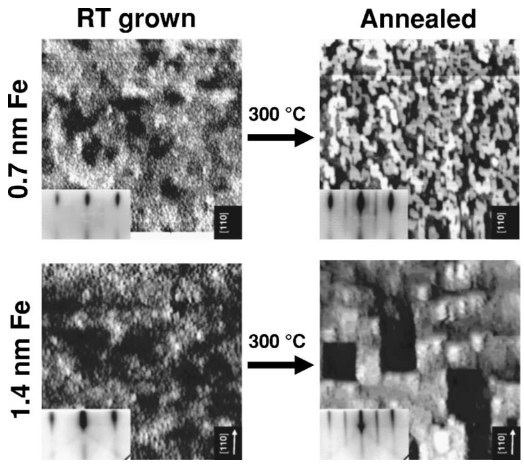

FIG. 4. STM images (200×200 nm^2) of the surface topography with the corresponding RHEED image for 0.7 nm (top) and 1.4 nm (bottom) Fe layers before and after a 300 °C anneal. The annealed Fe layers exhibit the ⟨110⟩ faceted features.

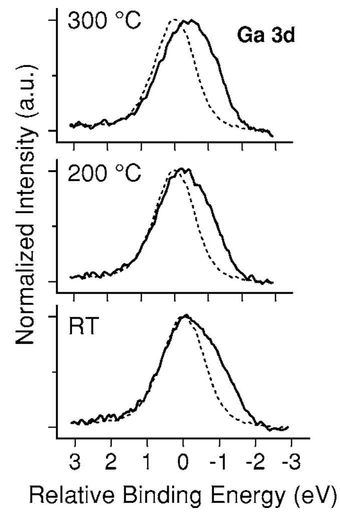

FIG. 5. XPS of the Ga 3*d* peak of 1.2 nm Fe layers for several annealing temperatures. For reference, the normalized Ga 3*d* peak from the bare GaAs surface is included as the dotted line.

STM analysis reveals the surface microstructure in more detail for these layers before and after a 300 °C anneal, as shown in Fig. 4 for 0.7 nm and 1.4 nm Fe layers. For both thicknesses, the initial RT deposited Fe layer is continuous across the surface. After annealing, the 0.7 nm Fe layer forms discrete island networks faceted along the ⟨110⟩ directions with regions of exposed GaAs consistent with the RHEED images. For the 1.4 nm layer, ⟨110⟩ faceted pits form deep enough to expose GaAs. Similar pit formation after annealing was previously reported in Fe/Cu(001) (Ref. 19) and Co/$Al_2O_3(11\bar{2}0)$.[20] The small angle of the electron beam in RHEED and the high aspect ratio of the pits would prevent diffraction of the GaAs exposed by these pits. The Fe region in between the pits flattens for the 1.4 nm Fe layer, which is consistent with the increased streaked quality of the RHEED pattern. X-ray reflectometry reveals a 16% increase in the Fe layer thickness after the 300 °C anneal consistent with the migration of Fe to form the pits.[16] Because the Fe tends to coalesce into the ⟨110⟩ faceted structures, we speculate that a reduction of the surface free energy is the driving force for this phenomenon instead of a mechanism such as strain relaxation or thermal expansion. The reduction of the surface free energy was also found to be responsible for the formation of faceted pits in annealed Fe layers grown on Cu(001) substrates.[20]

We performed XPS analysis using the Ga 3*d*, As 3*d*, Fe 2*p*, and Fe 3*p* emission lines to study the interfacial reaction occurring between the Fe layer and GaAs during annealing. The As 3*d*, Fe 2*p*, and Fe 3*p* emission peaks yielded no detectable difference for any thermal process. However, Fig. 5 shows the XPS spectra of the Ga 3*d* peak for the RT grown and 200 and 300 °C Fe layers. The Ga 3*d* peak taken from the bare (4×6) GaAs(001) surface prior to Fe deposition is also shown for reference in each spectrum as the dashed curve. As the Fe layer is deposited at RT, the Ga 3*d* peak exhibits a +0.8 eV shifted component, indicating the presence of Fe–Ga bonding.[21] This shifted component increases in relative intensity as the annealing temperature is increased. However, quantification of this increased Fe–Ga bonding is complicated by the microstructure, since STM revealed that there are two distinct chemical environments that we cannot resolve: the Fe layer and regions of exposed GaAs. The presence of exposed GaAs regions may also allow substrate species to migrate to the surface of the Fe layer, increasing the amount of Fe–Ga reaction. Such a migration is likely driven by lowering the surface free energy as with annealed Fe layers on Cu(001).[20]

Onset of ferromagnetism

The structural change that occurs during annealing has a significant effect on the magnetic behavior of the Fe layer. Figure 6 shows a plot of the spin-wave frequency as a function of the Fe layer thickness (d_{Fe}) along the easy [110] direction for RT deposited, 200 °C annealed, and 300 °C annealed Fe layers. A smoothed line through the data is included as a guide for the eyes. The critical thickness for the onset of ferromagnetism (d_{crit}) is taken as the point when the spin wave from a stable ferromagnetic phase vanishes, which we measure to be 0.45 nm for the RT Fe. Values of d_{crit} range from 0.38 to 1.5 nm in reports by other groups.[7–11,13] Re-

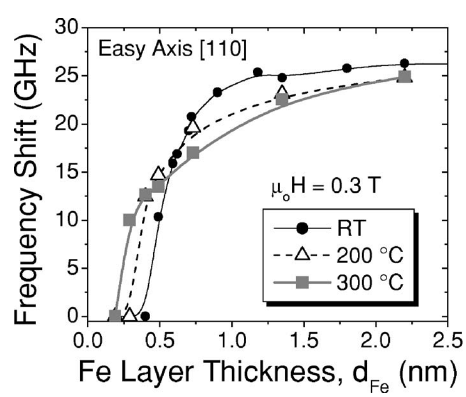

FIG. 6. The spin-wave frequency shift as a function of Fe layer thickness for RT as-deposited, 200 °C annealed, and 300 °C annealed conditions. BLS spectra were taken along the easy [110] axis with an applied field of 0.3 T. Smoothed lines are fitted through the data as a guide to the eyes.

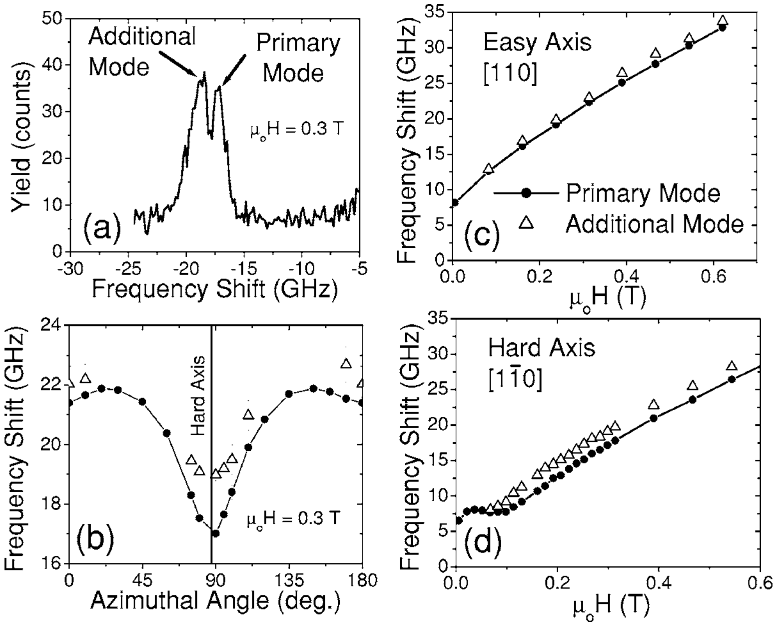

FIG. 7. BLS data from a 1.4 nm Fe layer annealed at 275 °C showing (a) a BLS spectrum illustrating the existence of two simultaneous spin-wave modes, (b) the angular dependence of the two modes, and [(c) and (d)], the field dependence of the two modes along the easy [110] and hard [1$\bar{1}$0] axes, respectively. The primary mode is indicated by the closed circles and the error bars are on the same size as the data points. The additional mode has significantly larger error bars and is indicated by the open triangles.

markably, d_{crit} decreases to 0.35 and 0.25 nm for Fe layers undergoing annealing at 200 and 300 °C, respectively. We believe that the increased ordering and coalescence of the Fe after annealing are responsible for the earlier transition to a ferromagnetic phase.

The lack of a ferromagnetic phase at Fe coverages below d_{crit} has previously been attributed to small Fe islands initially forming a superparamagnetic phase.[11,12] As more Fe is deposited these small islands coalesce forming a thermally stable ferromagnetic phase. In addition, there is evidence that initially the Fe layer is mostly disordered below d_{crit}, preventing the formation of a ferromagnetic phase.[10] Our results are consistent with both of these proposed mechanisms for the suppression of a ferromagnetic phase, since the Fe simultaneously coalesces into larger islands and orders with annealing.

Additional spin-wave mode

We previously reported the presence of an additional spin-wave mode in 1.0–1.5 nm Fe layers annealed above the critical annealing temperature of 225 °C.[16] A BLS spectrum of these simultaneous modes is shown in Fig. 7(a). The additional mode is at all times shifted higher in frequency relative to the primary spin-wave mode. The linewidth for the additional spin-wave mode is roughly twice that of the primary spin-wave mode which aids in identifying the two modes since they overlap substantially. The angular dependence of both spin-wave modes for a 275 °C annealed 1.4 nm Fe layer is shown in Fig. 7(b). The additional mode is primarily confined to the ⟨110⟩ axes, since the intensity decreases rapidly as the propagation direction is rotated away from one of these axes. The field dependences of the spin-wave modes along the easy [110] and hard [1$\bar{1}$0] axes are shown in Figs. 7(c) and 7(d), respectively.

The existence of the additional spin-wave mode correlates with the existence of pits in the Fe layer which occur only in the 1.0–1.5 nm range. For thicker annealed Fe layers, only the primary spin-wave mode is present and is consistent with the Fe layer being thick enough to remain continuous. For Fe layers below 1 nm in thickness, only a single mode exists even though the Fe layer is not continuous. However, the discontinuities of the network of islands in Fig. 4(b) are over an order of magnitude smaller than the pits shown in Fig. 4(a). The size scale of this network of islands is not large enough to contribute to the creation of an additional mode. Previous BLS observations of simultaneous spin-wave modes in ultrathin magnetic layers have attributed it to the formation of stripe domains[22,23] and in-plane structural twinned domains.[24] However, these results are inconsistent with our measurements. Recent ferromagnetic resonance (FMR) measurements and simulations of antidot (pit) arrays reveal that the dipole field created around an antidot induces an additional and spatially localized mode.[25,26] Since the angular and field dependences of these FMR modes are qualitatively similar to the additional spin-wave mode that we observe, and we only observe the additional mode when pits are present in the Fe layer, we conclude that a similar mechanism may be responsible for our results. This would also explain why only a single mode exists below 1 nm. In this case, the sizes of the discontinuities are too small and too closely spaced to establish a strong enough dipole field within a region large enough for long-wavelength spin-wave modes to exist. However, it is surprising that broader linewidths for the localized mode are not observed from a distribution of frequencies caused by the random pit spacing.

Magnetic properties

The existence of two simultaneous spin-wave modes complicates the fitting of our BLS data, since the error in extracting the additional mode was generally large and the strict confinement of the propagation directions to the ⟨110⟩ axes resulted in an incomplete data set for that mode. Therefore, we report only dynamic magnetic properties derived from fits to the primary nonlocalized spin-wave mode. Fig-

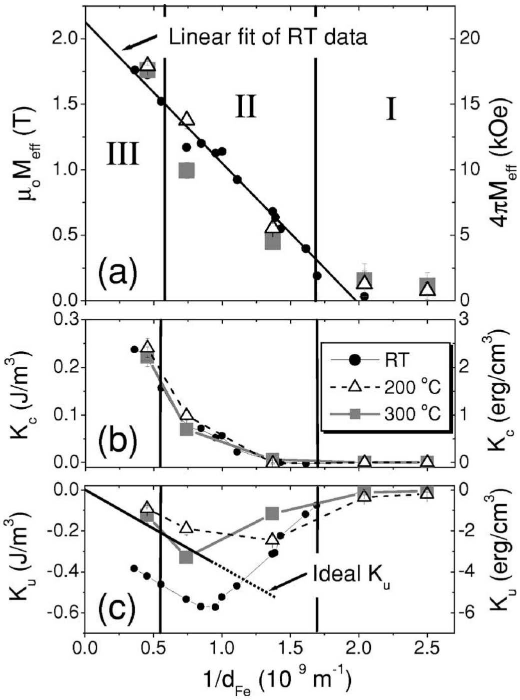

FIG. 8. Results from fits to our BLS data of (a) M_{eff}, (b) K_c, and (c) K_u for Fe layers undergoing various annealing processes as a function of the inverse Fe layer thickness. The data can be divided into three regions (marked I, II, and III) where trends in the annealed Fe data deviate from the RT as-deposited data.

ure 8(a) shows a plot of the effective magnetization (M_{eff}) versus the inverse Fe layer thickness ($1/d_{Fe}$) for the RT deposited, 200 °C annealed, and 300 °C annealed processes. For clarity, a regression line through the RT data is included, since the data display excellent linearity as expected for the relationship between M_{eff}, the saturation magnetization (M_s), and the out-of-plane surface anisotropy (K_{out}) given in Eq. (1):[6]

$$M_{eff} = DM_s - \frac{2K_{out}}{\mu_o M_s}\frac{1}{d_{Fe}}, \tag{1}$$

where $D=1-0.2338/n$ is the demagnetization factor and n is the number of monolayers of Fe.[27] We identify three thickness ranges (marked I, II, and III in Fig. 8) where M_{eff} changes relative to the RT deposited Fe. In region I ($d_{Fe} \leqslant 0.6$ nm), M_{eff} is significantly greater for both annealing temperatures. This increase in M_{eff} is due to the increased crystallization and coalescence in the Fe layer that occur during the annealing process and which are also responsible for the earlier onset of a ferromagnetic phase.

In region II ($0.6\ \text{nm} \leqslant d_{Fe} \leqslant 1.8$ nm), the value of M_{eff} for the 300 °C annealed layers is significantly lower than the RT Fe. We speculate that the formation of a discontinuous Fe microstructure and modified interface is the primary cause of the decrease in the overall value of M_{eff}. In addition, the increased reaction of Fe with substrate species or migration of substrate species to the surface may lower the total magnetic moment and also affect K_{out} in the Fe layer. Recall that XPS results showed a significant increase in Fe–Ga bonding following annealing.

The cubic anisotropy constant (K_c) is primarily a volume energy resulting from the bulk Fe magnetocrystalline anisotropy. This term, plotted in Fig. 8(b), shows no significant deviation from the RT data for all thicknesses. This further indicates that the change we observe in M_{eff} most likely originates at the interfaces. The 200 °C annealed layers do not exhibit a significant deviation in M_{eff} or K_c relative to the RT Fe. Recall that 200 °C annealed layers in this thickness range do not undergo a significant change in microstructure that would expose GaAs. Therefore, the migration of substrate species to the surface and interfacial reaction is decreased.

However, the behavior of the uniaxial anisotropy constant (K_u) is considerably different after annealing, as shown in Fig. 8(c). K_u is known to be primarily interfacial in origin[6,9,10] and is therefore susceptible to the quality or chemical nature of the interface. Thus, increased interfacial reaction will modify the surface anisotropy. In addition, as the Fe coalesces and leaves behind regions of exposed GaAs, the surface area of the interface itself is decreased further resulting in a reduction of K_u. This effect would be significant only in the thinner Fe layers where the regions of exposed GaAs are a significant fraction of the total surface area. However, we have recently shown that RT Fe layers with Al overlayers have a significant volume component to K_u due to anisotropic strain resulting from the 1.4% lattice mismatch between Fe and GaAs and the influence of the Al overlayer.[18] The relationship between the surface (K_u^{surf}) and volume (K_u^{vol}) components of K_u are given in Eq. (2), where the factor of 2 arises due to there being two interfaces:

$$K_u = K_u^{vol} + \frac{2}{d_{Fe}}K_u^{surf}. \tag{2}$$

This anisotropic strain results in a $-0.25\ \text{J/m}^3$ (-2.5 erg/cm^3) offset in K_u for Fe layers greater than 1.1 nm representing the thickness range where K_u vs $1/d_{Fe}$ is linear and Eq. (1) applies. We have included in Fig. 8(c) a line corresponding to the expected behavior of K_u for RT Fe without the anisotropic strain induced component (i.e., $K_u^{vol}=0$). Above 1.1 nm, the 300 °C annealed data are in much better agreement with this line. This is strong evidence that the annealing process induces an isotropic relaxation in the Fe layer. Also, the coercive field decreases with annealing temperature prior to pit formation, further indicating a relaxation and reduction of defects upon annealing.[16] However, it is likely that a combination of this relaxation, interfacial reaction, and reduction of interfacial surface area contributes to the total reduction in K_u.

Finally, in Fe layers thicker than 1.8 nm (region III), the values of M_{eff} are equivalent for all three processing conditions. At these thicknesses, pit formation no longer occurs in the 300 °C annealed layers, and therefore the properties are no longer influenced by such discontinuities in the structure. This is significant because we observe M_{eff} to deviate from the RT Fe data only in the thickness region where the Fe layer is discontinuous. Thus, the presence of these discontinuities must be responsible, either directly or indirectly, for the reduction of M_{eff} through a reduced interfacial surface area, shape effects, or migration of substrate species to the surface and subsequent reaction.

CONCLUSIONS

We have determined the effect annealing up to 300 °C has on the structure, spin dynamics, and magnetic properties in epitaxial Fe layers grown on GaAs. The resulting structure of the Fe layer has a profound effect on the spin dynamics and magnetic properties. The formation of a discontinuous Fe layer causes the formation of simultaneous spin-wave modes and contributes to a reduction in the magnitudes of M_{eff} and K_u. A further reduction in K_u also results from a relaxation in the Fe layer that occurs during the annealing process. In addition, the critical thickness for the onset of a ferromagnetic phase can be significantly reduced by the coalescence and ordering that occur during annealing. Although we present strong evidence that interfacial reaction, crystalline relaxation, and the Fe layer microstructure are responsible for the observed changes in magnetic properties, more work is needed to separate and quantify the individual contributions.

ACKNOWLEDGMENTS

We are grateful to Sungkyun Park, Sukmock Lee, Pavel Kabos, and Tom Silva for their advice and valuable discussions; Ross Potoff for his technical support; and Barry Wilkens for conducting Rutherford backscattering spectrometry measurements used to calibrate deposition rates. This work is partially supported by ONR/DARPA N00014-02-01-0627. This work is a contribution of the National Institute of Standards and Technology and is not subject to copyright.

[1] J. J. Krebs, B. T. Jonker, and G. A. Prinz, J. Appl. Phys. **61**, 2596 (1987).
[2] M. Ramsteiner, H. J. Zhu, H.-P. Schönherr, and K. H. Ploog, Physica E (Amsterdam) **13**, 529 (2002).
[3] A. F. Isakovic, D. M. Carr, J. Strand, B. D. Schultz, C. J. Palmstrøm, and P. A. Crowell, J. Appl. Phys. **91**, 7261 (2002).
[4] J. Strand, B. D. Schultz, A. F. Isakovic, C. J. Palmstrøm, and P. A. Crowell, Phys. Rev. Lett. **91**, 036602 (2003).
[5] X. Lou, C. Adelmann, M. Furis, S. A. Crooker, C. J. Palmstrøm, and P. A. Crowell, Phys. Rev. Lett. **96**, 176603 (2006).
[6] T. L. Monchesky, B. Heinrich, R. Urban, K. Myrtle, M. Klaua, and J. Kirschner, Phys. Rev. B **60**, 10242 (1999).
[7] M. Gester, C. Daboo, R. J. Hicken, S. J. Gray, A. Ercole, and J. A. C. Bland, J. Appl. Phys. **80**, 347 (1996).
[8] E. M. Kneedler, B. T. Jonker, P. M. Thibado, R. J. Wagner, B. V. Shanabrook, and L. J. Whitman, Phys. Rev. B **56**, 8163 (1997).
[9] M. Madami, S. Tacchi, G. Carlotti, G. Gubiotti, and R. L. Stamps, Phys. Rev. B **69**, 144408 (2004).
[10] F. Bensch, R. Moosbühler, and G. Bayreuther, J. Appl. Phys. **91**, 8754 (2002).
[11] Y. B. Xu, E. T. M. Kernohan, D. J. Freeland, M. Tselepi, and J. A. C. Bland, Phys. Rev. B **58**, 890 (1998).
[12] S. J. Steinmuller, M. Tselepi, V. Strom, and J. A. C. Bland, J. Appl. Phys. **91**, 8679 (2002).
[13] G. W. Anderson, M. C. Hanf, X. R. Qin, P. R. Norton, K. Myrtle, and B. Heinrich, Surf. Sci. **346**, 145 (1996).
[14] B. Lépine *et al.*, J. Appl. Phys. **83**, 3077 (1998).
[15] F. P. Zhang, P. S. Xu, E. D. Lu, H. Z. Guo, F. Q. Xu, and X. Y. Zhang, Thin Solid Films **375**, 64 (2000).
[16] J. M. Shaw, S. Park, and C. M. Falco, J. Appl. Phys. **95**, 6552 (2004).
[17] J. M. Shaw and C. M. Falco, J. Magn. Magn. Mater. **286**, 420 (2005).
[18] J. M. Shaw, S. Lee, and C. M. Falco, Phys. Rev. B **73**, 094417 (2006).
[19] H. T. Shi and D. Lederman, Phys. Rev. B **58**, R1778 (1998).
[20] J. Shen, J. Giergiel, A. K. Schmid, and J. Kirschner, Surf. Sci. **328**, 32 (1995).
[21] M. W. Ruckman, J. J. Joyce, and J. H. Weaver, Phys. Rev. B **33**, 7029 (1986).
[22] A. Murayama, K. Hyomi, J. Eickmann, and C. M. Falco, J. Magn. Magn. Mater. **198–199**, 372 (1999).
[23] M. G. Pini, P. Politi, A. Rettori, G. Carlotti, G. Gubbiotti, M. Madami, and S. Tacchi, Phys. Rev. B **70**, 094422 (2004).
[24] F. Scheurer, R. Allenspach, P. Xhonneux, and E. Courtens, Phys. Rev. B **48**, 9890 (1993).
[25] C. Yu, M. J. Pechan, and G. J. Mankey, Appl. Phys. Lett. **83**, 3948 (2003).
[26] M. J. Pechan, C. Yu, R. L. Compton, J. P. Park, and P. A. Crowell, J. Appl. Phys. **97**, 10J903 (2005).
[27] B. Heinrich, J. F. Cochran, M. Kowalewski, J. Kirschner, Z. Celinski, A. S. Arrott, and K. Myrtle, Phys. Rev. B **44**, 9348 (1991).